ACS OMEGA

Open Access

http://pubs.acs.org/journal/acsodf

Article

Study on the Synergistic Effect of SiO_2 and H_2O on Oxidative Coupling of Methane over Mn−Na_2WO_4/SiO_2 Catalyst

Qingjing Liu, Ruisheng Wang, Ranjia Li, Xiaosheng Wang, Suoqi Zhao, and Changchun Yu*

Cite This: *ACS Omega* 2024, 9, 36751−36760

Read Online

ACCESS | Metrics & More | Article Recommendations

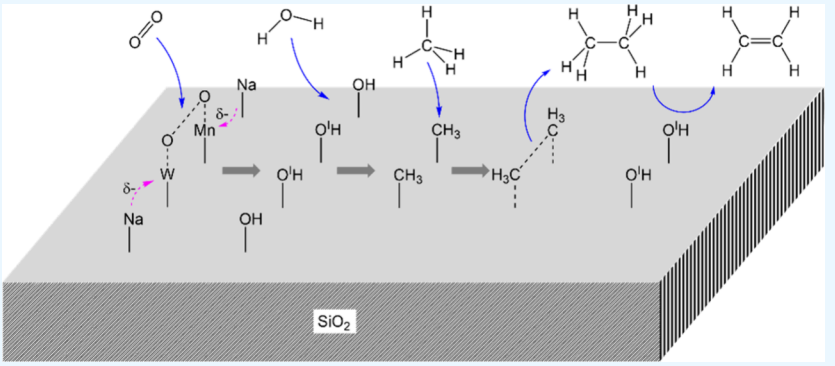

ABSTRACT: Mn−Na_2WO_4-based catalysts with different supports were prepared using the incipient wetness impregnation method and evaluated for their oxidative coupling of methane (OCM) reaction performance. The results demonstrated that the SiO_2- supported catalyst exhibited the best catalytic performance, and the introduction of H_2O further enhanced its activity. Under the conditions of a feed gas mixture of $CH_4/O_2/H_2O$ = 6:1:24 at 800 °C and atmospheric pressure, the CH_4 conversion and C_{2+} selectivity over the Mn−Na_2WO_4/SiO_2 catalyst increased from 28.4% and 77.4% (without H_2O) to 33.2% and 84.9%, respectively. In contrast, the catalytic activity using TiO_2 and MgO supports drastically declined. Characterizations using X-ray diffraction (XRD), *in situ* infrared spectroscopy (*In-situ* IR), X-ray photoelectron spectroscopy (XPS), hydrogen temperature-programmed reduction (H_2-TPR), and oxygen temperature-programmed desorption (O_2-TPD) revealed that the introduction of steam not only served as a diluent to decrease the partial pressures of the reactants CH_4 and O_2, thereby reducing deep oxidation reactions in the gas phase, but also interacted with surface oxygen species (O_2^{2-}) and silica to form adjacent surface-bonded disilanol free radicals Si−O^{1}H. This interaction facilitated the dehydrogenation and coupling of two methane molecules on the catalyst surface, resulting in the generation of C_{2+} products, significantly enhancing the catalytic activity and selectivity of OCM.

1. INTRODUCTION

The oxidative coupling of methane (OCM) reaction is an efficient method for the one-step production of ethylene from CH_4. Since the pioneering work by Keller and Bhasin from the Union Carbide Corporation (UCC) in 1982,[1] the OCM reaction has gained significant attention from the scientific community and industrial community. Researchers have selected and tested thousands of catalysts and extensively studied their reaction mechanisms, yet achieving the industrially desired single-pass yield of 30% for C_{2+} species remains challenging. The main issue with the OCM reaction is that both the feedstock CH_4 and the product C_{2+} species are prone to deep oxidation to CO or CO_2 during the conversion process, which reduces the selectivity for C_{2+} products.[2−4]

Among the currently developed OCM catalysts, the Mn−Na_2WO_4/SiO_2 catalyst, first proposed by the Lanzhou Institute of Chemical Physics (LICP), is considered to have the most industrial potential due to its relatively high CH_4 conversion (20−30%) and C_{2+} selectivity (70−80%).[5−8] To further enhance the catalytic performance of the Mn−Na_2WO_4/SiO_2 catalyst, researchers have focused on various aspects such as catalyst preparation methods,[9,10] promoter modification,[9,11] process condition optimization,[12,13] and reaction mechanisms,[14,15] with particular emphasis on the active sites of the catalyst. Ji et al.[16] proposed that the Na−O−Mn and Na−O−W sites are the active sites for CH_4 activation, with Na−O−Mn mainly present on the surface of the catalyst and Na−O−W located deeper within the catalyst. Li et al.[17,18] suggested

Received: June 14, 2024
Revised: July 19, 2024
Accepted: August 9, 2024
Published: August 17, 2024

that the active site responsible for CH_4 activation consists of a WO_4 tetrahedral species composed of one W═O bond and three W−O−Si bonds. They revealed that CH_4 is activated at the W^{6+}/W^{5+} active site, while O_2 is activated at the Mn^{3+}/Mn^{2+} active site. Wachs et al.[19−22] proposed, through *in situ* Raman, TAP, and DFT calculations, that highly dispersed Na-WO_x is the active-selective site. Sinev et al.[23] studied the redox behavior on the MnO_x−Na_2WO_4/SiO_2 catalyst, showing that Na_2WO_4 crystals and Mn_2O_3 phases disappear during oxygen temperature-programmed desorption, forming $MnWO_4$ and a gel-like substance. Schomäcker et al.[24,25] demonstrated the importance of the "$Mn^{3+} \leftrightarrow Mn^{2+}$" redox cycle. Takanabe and Iglesia et al.[26,27] found that H_2O catalytically promotes the formation of C_{2+} during the reaction because H_2O and O_2 form hydroxyl radicals (OH·) on Na_2WO_4, which in turn inhibits the deep oxidation of methane to CO/CO_2.

Despite extensive research on the Mn−Na_2WO_4/SiO_2 catalyst, there are still controversies regarding the catalytic properties, active sites, and corresponding reaction mechanisms of components in the OCM process, particularly the role of the SiO_2 support. Current studies mainly focus on its transformation from amorphous SiO_2 to the α-cristobalite phase at low temperatures under the influence of Na during the calcination of the catalyst precursor, facilitating the surface enrichment of W and Mn during SiO_2 crystallization and uniformity of the tetrahedral WO_4 structure.[28,29] To further understand the role of the SiO_2 support, this study prepared a series of Mn−Na_2WO_4 based catalysts with different supports. Catalyst performance evaluations revealed that the introduction of a high concentration steam into the feed gas significantly decreased the activity of TiO_2 and MgO supported catalysts, whereas both the activity and C_{2+} selectivity of the SiO_2 supported catalyst significantly improved. Consequently, it is hypothesized that the SiO_2 support has a synergistic effect on the OCM process. A series of characterization analyses and validations were conducted to explain the synergistic promotion effect of SiO_2 and H_2O on the OCM reaction over the Mn−Na_2WO_4/SiO_2 catalyst.

2. EXPERIMENTAL SECTION

2.1. Catalyst Preparation. SiO_2 (Qingdao Marine Chemical Company), TiO_2 (Beijing Chemical Reagent Company), and MgO (China National Pharmaceutical Group Chemical Reagent Co., Ltd.) were used as supports. $Mn(NO_3)_2$ (China National Pharmaceutical Group Chemical Reagent Co., Ltd.), $Na_2WO_4{\cdot}2H_2O$ (Aladdin Reagent (Shanghai) Co., Ltd.), and citric acid (Beijing Chemical Reagent Company) were used as the raw materials to prepare the catalysts via the incipient wetness impregnation method. The required amounts of $Mn(NO_3)_2$, $Na_2WO_4{\cdot}2H_2O$, and citric acid were calculated based on the loading amount and the mass of the support and then dissolved in water to prepare the impregnation solution. Both the support and the impregnation solution were preheated to 80 °C; the support was then quickly mixed with the impregnation solution. The resulting solid was dried at 120 °C for 6−8 h, followed by calcination in a muffle furnace under an air atmosphere, heating at a rate of 1.5 °C/min to 850 °C and maintaining this temperature for 8 h. After cooling to room temperature, the solid was sieved to obtain 20−40 mesh particles, resulting in catalysts with loadings of 2.15 wt % Mn and 5.4 wt % Na_2WO_4 on different supports, as shown in Table 1.

Table 1. Abbreviation of the Mn−Na_2WO_4 Based Catalysts with Different Support

Catalyst	Abbreviation
Mn−Na_2WO_4/SiO_2	MNWS
Mn−Na_2WO_4/TiO_2	MNWT
Mn−Na_2WO_4/MgO	MNWM

2.2. Catalytic Performance Evaluation. The performance tests of the OCM catalysts were conducted at atmospheric pressure using a micro fixed-bed reactor. A quartz tube with an inner diameter of 6 mm was used as the reactor, which was placed vertically in an electric heating furnace. The catalyst bed was located in the constant temperature zone of the furnace. The amount of catalyst loaded was 0.375 g with a bed thickness of approximately 35 mm. Quartz wool was filled at both ends of the catalyst bed, and quartz sand was filled from the lower quartz wool to the reactor outlet for the support. The outlet at the lower end of the reactor was supported with a stainless steel wire mesh. The feed gas and product gas were analyzed by a Fuli GC9790II gas chromatography equipment with TCD and FID detectors. The TCD detector was operated at temperature of 110 °C, H_2 as carrier gas, a Φ 2 mm × 1829 mm Shincarbon ST column used for analysis of O_2, CH_4, C_2H_6, C_2H_4, C_3H_8, C_3H_6, CO, CO_2, N_2. The FID detector was operated at temperature of 200 °C, N_2 as carrier gas, a Φ 2 mm × 2000 mm Porapak QS column used for light hydrocarbons analysis, including CH_4, C_2H_4, C_2H_6, C_{3+}, etc.

2.3. Characterization. XRD was analyzed on a Bruker D8 Advance diffractometer. The analysis conditions were: Cu Kα radiation, Ni filter, X-ray tube voltage 40 kV, current 40 mA, LynxEye array detector, scan step 0.025°, scan speed 4°/min, and scan range 5−90°.

XPS was performed on a Thermo Escalab 250Xi spectrometer. The analysis conditions were: Al Kα source with 14.8 kV and 1.6 A, 650 μm beam spot, charge compensation using a low-energy electron flood gun, and charge correction with C 1s = 284.8 eV. The high-resolution scan has a pass energy of 20 eV and step size of 0.1 eV.

In situ IR was carried out on a Bruker 80 V infrared spectrometer using a DTGS detector, The transmission method was used with a wavenumber range of 4000−400 cm^{-1} and scan step of 4 cm^{-1}.

H_2-TPR and O_2-TPD were performed on self-built temperature-programmed system equipment with a Pfeiffer QMG220 quadrupole mass spectrometer as an online detector and a catalyst loading of 400 mg. The catalyst was predegassed at 450 °C for 30 min and cooled to 100 °C in Ar flow. H_2-TPR was conducted at a ramp rate of 10 °C/min in a 30 mL/min 10 vol % H_2/Ar flow; and O_2-TPD was conducted at a ramp rate of 10 °C/min in a 30 mL/min He flow. The QMS operated in a multiple ion detection (MID) mode with a sample rate of 10 Hz, and the main mass spectrum signals detected were m/z = 2 (H_2), m/z = 18 (H_2O), and m/z = 32 (O_2).

3. RESULTS AND DISCUSSION

3.1. The OCM Reaction Performance of Different Supported Catalysts. The three as-prepared catalysts were examined in the OCM reaction using a CH_4 gas hourly space velocity of 8000 $mL{\cdot}g_{cat.}^{-1}{\cdot}h^{-1}$ for a feed gas of CH_4/O_2= 6:1 (molar ratio) at 800 °C and atmospheric pressure for 4 h (shown as Figure 1(a)). The catalyst MNWS exhibited a CH_4

https://doi.org/10.1021/acsomega.4c05565
ACS Omega 2024, 9, 36751−36760

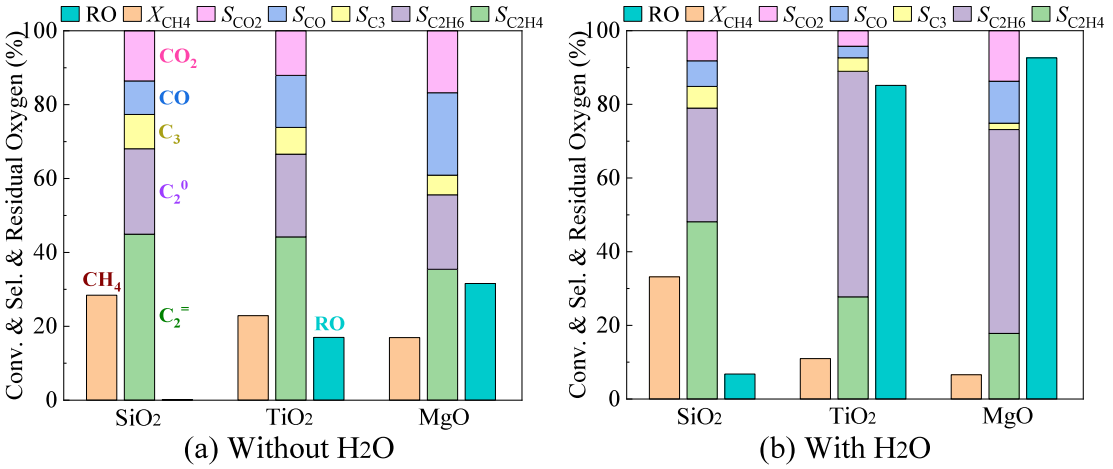

Figure 1. Catalytic performance obtained from steady-state OCM experiments of the catalysts with different support. Reaction condition: $W_{cat.}$ = 0.375 g, T = 800 °C, 0.1 MPa, $GHSV_{(CH4)}$ = 8000 mL·$g_{cat.}^{-1}$·h^{-1}, CH_4: O_2: H_2O = 6:1: x (a, x = 0; b, x = 24). RO: Residual Oxygen, RO = amount of oxygen in product gas/amount of oxygen in feed gas ×100%.

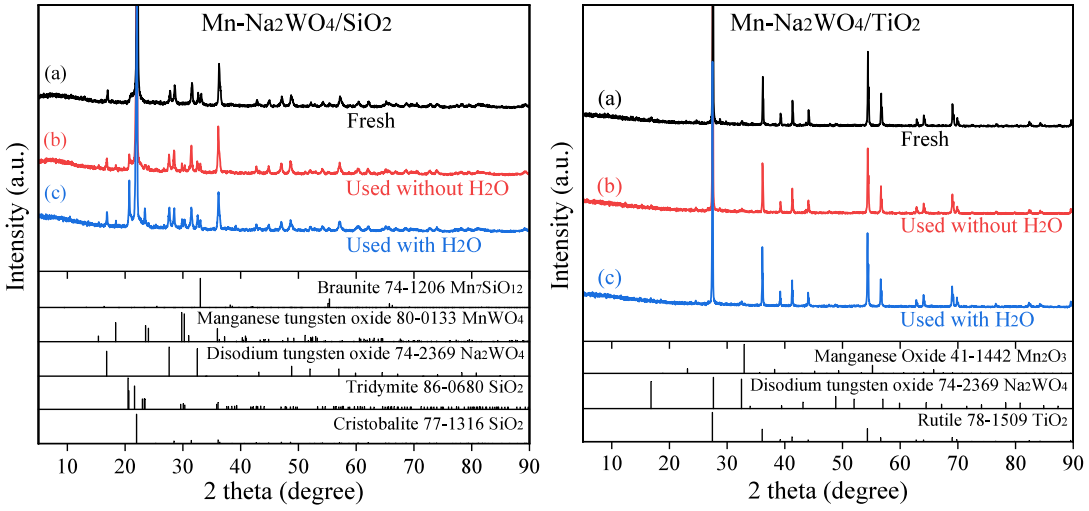

Figure 2. XRD patterns of the catalyst Mn−Na_2WO_4/SiO_2 and Mn−Na_2WO_4/TiO_2 (a) fresh, (b) used without H_2O, (c) used with H_2O.

conversion of 28.4% and a C_{2+} selectivity of 77.4%, with a residual oxygen content of 0.2%, demonstrating the highest CH_4 conversion and C_{2+} selectivity. The next best catalyst was MNWT, with a CH_4 conversion of 22.9%, a C_{2+} selectivity of 73.8%, and a residual oxygen content of 17.0%. Among the three catalysts, MNWM showed the poorest OCM performance, with a CH_4 conversion of 16.9%, a C_{2+} selectivity of 60.9%, and a residual oxygen content of 31.6%.

With the same reaction conditions, the introduction of steam into the feed gas with a $CH_4/O_2/H_2O$ molar ratio of 6:1:24 was used to further investigate the OCM performance of these three catalysts (shown as Figure 1(b)). Comparison with the conditions without steam revealed that for the catalyst MNWS, the CH_4 conversion increased from 28.4% to 33.2%, the C_{2+} selectivity increased from 77.4% to 84.9%, and the residual oxygen content increased from 0.15% to 6.8%. Both the catalytic activity and selectivity were significantly improved. The increased activity and selectivity, along with reduced oxygen consumption, directly indicate a significant enhancement in the selective oxidation of low oxygen consumption and a substantial reduction in the deep oxidation of high oxygen consumption.

For the catalyst MNWT, the CH_4 conversion substantially decreased from 22.9% to 11.0%, the C_{2+} selectivity increased from 73.8% to 92.6%, and the residual oxygen sharply increased from 17.0% to 85.0%. The catalyst MNWM showed a trend similar to that of MNWT, with the CH_4 conversion substantially decreased from 16.9% to 6.6%, the C_{2+} selectivity increasing significantly from 60.9% to 74.9%, and the residual oxygen sharply increased from 31.6% to 92.6%.

From the comparison of evaluation results, the performance of these three catalysts with and without the introduction of steam is quite different. Under both reaction conditions, the catalyst MNWS exhibited the best OCM performance with very low residual oxygen content. After introducing steam, both the CH_4 conversion and C_{2+} selectivity of MNWS significantly increased. In contrast, the CH_4 conversions of catalysts MNWT and MNWM substantially decreased after introducing steam, although their C_{2+} selectivity increased in different degrees. It should be noted that the residual oxygen of both MNWT and MNWM increased sharply, indicating that the introduction of steam greatly hindered the activation and conversion of oxygen, resulting in a substantial decrease in the CH_4 conversion.

https://doi.org/10.1021/acsomega.4c05565
ACS Omega 2024, 9, 36751−36760

Table 2. Thermodynamic Parameters of the Two New Crystal Phases Formation of Catalyst MNWS under 800 °C

No.[a]	Reaction	$\Delta G_{800°C}$ (kJ/mol)	$\Delta H_{800°C}$ (kJ/mol)
1	SiO_2(Cristobalite) = SiO_2(Tridymite)	−0.1	−1.0
2	$Na_2WO_4 + MnO + SiO_2 = MnWO_4 + Na_2SiO_3$	−109.4	105.2

[a]1. Cristobalite SiO_2 to Tridymite SiO_2; 2. Under steam condition

3.2. The Characterization of Catalysts. According to the catalytic performance of the three catalysts, the MNWT and MNWM catalysts showed very similar trends and results in the variation of the CH_4 conversion, C_{2+} selectivity, and residual oxygen, both of which were significantly different with the MNWS catalyst. TiO_2 and SiO_2 are both dioxides with the same valence. To elucidate the difference in the performance of the OCM after the introduction of steam, the catalysts MNWS and MNWT were selected for characterization before and after the reaction.

Figure 2 shows the XRD patterns of the catalysts before and after reaction evaluation. XRD analysis showed significant differences before and after the reaction evaluation. For the MNWT, rutile TiO_2 and Na_2WO_4 diffraction peaks can be observed before and after the reaction evaluation, with no Mn_2O_3 or other manganese oxide phases detected, and no significant changes in the diffraction peaks' intensity before and after the reaction evaluation. In contrast, the MNWS showed significant differences before and after reaction evaluation. Distinct α-cristobalite, Na_2WO_4, and Mn_7SiO_{12} diffraction peaks are observed in the fresh MNWS. After the reaction evaluation, new crystalline phases of tridymite and $MnWO_4$ appear, and the diffraction peaks' intensity of the tridymite phase are significantly enhanced after the introduction of steam. These results indicate that significant chemical reactions occur over the MNWS during the evaluation, especially when steam is introduced to the feed gas. Under high temperature and high steam concentration conditions, the MNWS undergoes significant hydrothermal crystallization, leading to the formation of new crystalline phases. This suggests that high temperature, H_2O, and SiO_2 play important roles in the formation of the new crystalline phases in MNWS. Thermodynamic calculations indicate that the conversion of α-cristobalite to tridymite at 800 °C, and the formation of $MnWO_4$ from Na_2WO_4 and MnO in the presence of SiO_2, are thermodynamically favorable (Table 2). XRD shows that the intensity of the tridymite phase diffraction peaks is much higher under high steam conditions, suggesting that a higher concentration of steam under the high-temperature condition is more favorable for the formation of the tridymite phase. These results confirm that there is a synergistic effect between SiO_2 and H_2O in MNWS, with the presence of H_2O significantly promoting the formation of the new crystalline phase tridymite.

At a high temperature of 800 °C, the thermodynamic parameters for the hydrated hydroxylation reactions of cristobalite phase SiO_2, rutile phase TiO_2, and MgO with H_2O to form the corresponding surface hydroxyl compounds were calculated and are presented in Table 3. The Gibbs free energy values for these hydrated hydroxylation reactions at 800 °C indicate that only the reaction involving SiO_2 is thermodynamically favorable. This finding provides theoretical support for the reaction between SiO_2 and H_2O at high temperatures, thereby suggesting that SiO_2 can synergistically promote the oxidative coupling of methane.

Table 3. Thermodynamic Parameters of Surface Hydroxyl Formation by Support Hydration under 800 °C

No.[a]	Reaction	$\Delta G_{800°C}$ (kJ/mol)	$\Delta H_{800°C}$ (kJ/mol)
1	$SiO_2 + H_2O + OH^- = SiO(OH)_3^-$[30]	−429.2	1648.2
2	$TiO_2 + H_2O = TiO(OH)_2$[31]	582.0	−46.8
3	$MgO + H_2O = Mg(OH)_2$[32]	366.9	−149.3

[a]1. Cristobalite SiO_2; 2. Rutile TiO_2

For the catalysts MNWT and MNWM, thermodynamic analysis indicates that the hydrated hydroxylation of both TiO_2 and MgO is quite unfavorable. When a high-concentration steam is introduced, H_2O primarily adsorbs on the catalyst surface, covering the surface W and Mn sites. This coverage effectively isolates and blocks the adsorption and activation of oxygen on the catalyst's active sites. Consequently, this leads to a significant decrease in catalyst activity and a substantial increase in residual oxygen levels. These results imply that SiO_2 in the MNWS plays a crucial role in gas-phase oxygen activation during the OCM reaction. The activation and conversion of gas-phase molecular oxygen are closely related to the synergistic effect of the support. Without this synergistic effect, even with a large amount of oxygen at high temperatures, activation and conversion would not occur. Additionally, for the catalysts MNWT and MNWM, after the introduction of steam, H_2O not only adsorbs on the catalyst surface, inhibiting the OCM reaction by partially blocking surface active sites, but also isolates and reduces noncatalytic oxidation reactions of CH_4 and C_{2+} products with gas-phase molecular oxygen. This results in a significant increase in the C_{2+} selectivity and a substantial increase in residual oxygen.

To further confirm that H_2O and SiO_2 indeed undergo high-temperature hydrated hydroxylation, forming surface silanol structures (Si−OH), *in situ* IR with vacuum temperature-programmed desorption (TPD) was conducted on the postreaction catalyst MNWS. After reacting for 4 h under conditions of 800 °C, atmospheric pressure, $CH_4/O_2/H_2O$ = 6:1:24, and a CH_4 hourly space velocity of 8000 $mL \cdot g_{cat.}^{-1} \cdot h^{-1}$, the MNWS catalyst was cooled to 120 °C while maintaining the reaction atmosphere. At 120 °C, the O_2 and H_2O feed was stopped, and the temperature was held for 10 min before cooling to room temperature. The MNWS sample was then pressed as an Φ 13 mm disc and transferred to an IR spectrometer for temperature-programmed *in situ* IR analysis.

The results are shown in Figure 3. Figure 3(a) presents the IR spectrum measured at room temperature and atmospheric pressure. The sample cell was then evacuated to 1.6×10^{-5} mbar, and the spectrum in Figure 3(b) was obtained. The sample was subsequently heated under vacuum at a rate of 5 °C/min up to 400 °C, with spectra recorded at various temperatures (Figure 3(c−g)). After holding at 400 °C for 30 min, the sample was allowed to cool naturally to 30 °C, and the spectrum in Figure 3(h) was recorded.

https://doi.org/10.1021/acsomega.4c05565
ACS Omega 2024, 9, 36751−36760

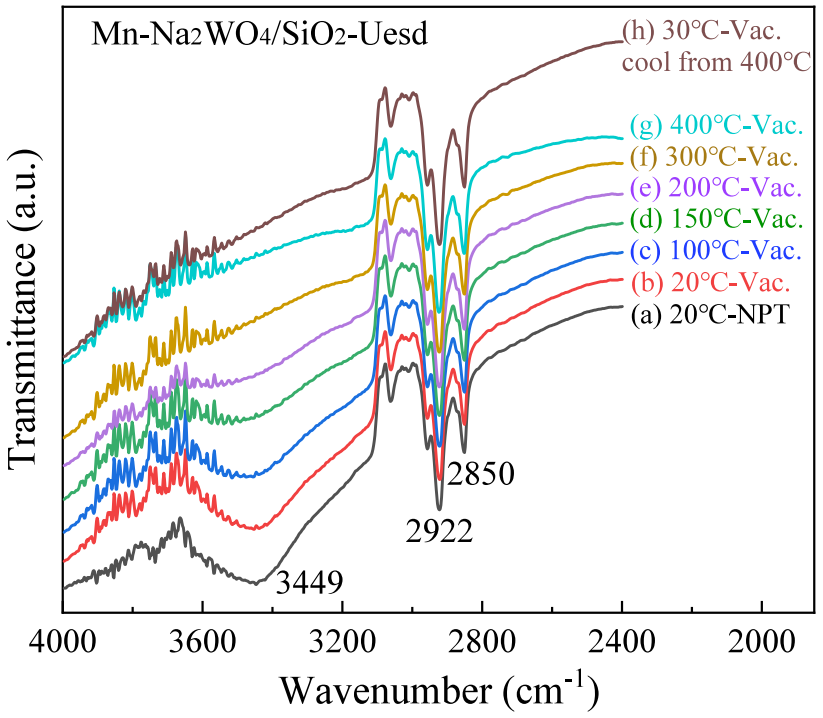

Figure 3. IR spectra of the Mn−Na_2WO_4/SiO_2 catalyst after being used with H_2O. *NPT*: normal pressure and temperature; Vac.: vacuum.

At 2850 and 2922 cm^{-1}, absorption peaks corresponding to Na_2WO_4 were observed, while the broad peak at 3449 cm^{-1} was attributed to the asymmetric stretching vibrations of hydroxyl groups on the SiO_2 surface. Comparing Figure 3(a), (b), there was a slight change in the hydroxyl peak at 3449 cm^{-1} after evacuation, indicating that the hydroxyl groups on the catalyst surface were not derived from weakly adsorbed water, which can be removed by vacuum treatment. As the temperature increased, the absorbance of hydroxyl groups on the catalyst surface gradually decreased, indicating dehydroxylation. The hydroxyl absorbance disappeared completely at 300 °C. After heating to 400 °C and holding for 30 min, then cooling to room temperature, no hydroxyl absorption peak reappeared.

The *in situ* IR results show that significant silanol groups (Si−OH) were present on the catalyst surface after the evaluation under steam conditions. These silanol groups did not reappear upon cooling to room temperature after being removed by heating samples under a vacuum, indicating that the formation of silanol groups through the reaction of SiO_2 and H_2O is a reversible process. At higher temperatures, the silanol groups condense and dehydrate. During the dehydroxylation process, when the temperature exceeds 190 °C, adjacent silanol groups condense, releasing H_2O molecules and causing the disappearance of the silanol groups' absorbance. At temperatures above 500 °C, only isolated single silanol groups can exist on the surface.[33,34] For the used MNWS catalyst, the silanol absorption peak at 3449 cm^{-1} disappeared completely at around 300 °C under vacuum, indicating that SiO_2 and H_2O primarily form adjacent disilanol groups on MNWS under experimental temperatures, which easily undergo dehydration reactions and disappear. This suggests a dynamic equilibrium of continuous formation and desorption of adjacent disilanol groups on the catalyst surface under conditions of steam and a temperature of 800 °C, as shown below:

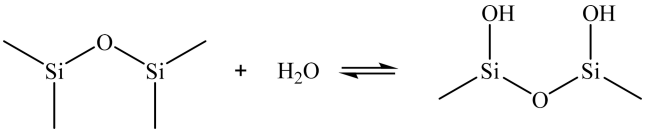

Due to the interaction between H_2O and SiO_2, the surface structure of the support becomes unstable, driving the system toward the formation of new crystalline phases with lower free energy. This promotes the generation of new crystalline phases, resulting not only in the conversion of part of SiO_2 from the α-cristobalite phase to the tridymite phase, but also in the formation of the $MnWO_4$ crystalline phase (Figure 2, Table 2).

XPS characterization was performed on the fresh and used (with H_2O) MNWS and MNWT catalysts. The high-resolution scan spectra for both catalysts are shown in Figure 4, and the binding energies, assignments, and surface atomic concentrations of each element are provided in Table 4 (MNWS) and Table 5 (MNWT). Significant differences in the surface element content between the MNWS and MNWT were observed.

The surface of MNWS has a high Si surface atomic concentration exceeding 20 at. %, followed by a relatively high Na surface atomic concentration, while the surface W and Mn atomic concentration are quite low. In contrast, the surface of MNWT contains Ti and Na between 10 and 20 at. %, with the surface W content being about twice that of MNWS, and the surface Mn atomic concentration is similar to that of MNWS. No significant chemical shifts in the binding energies of the main elements on the surface of MNWS and MNWT were observed before and after the reaction evaluation, indicating that the valence states of the elements did not change significantly. The presence of distinct Mn 2p satellites in both catalysts before and after the reaction suggests that Mn exists mainly as Mn^{2+}, which may be the primary electron-donating active site for the activation of molecular oxygen.

https://doi.org/10.1021/acsomega.4c05565
ACS Omega 2024, 9, 36751−36760

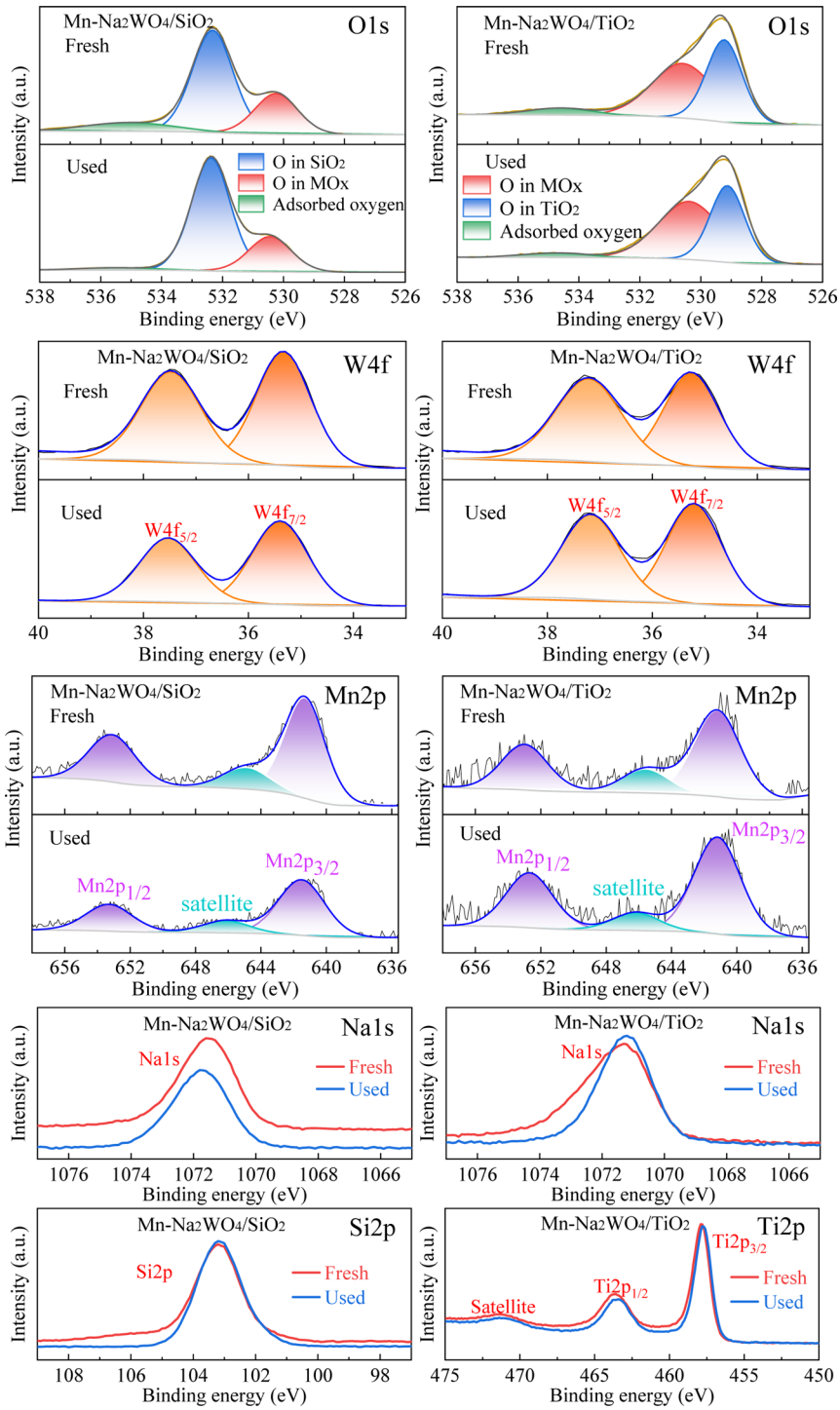

Figure 4. XPS spectra of the fresh and used (with H_2O) catalysts of Mn−Na_2WO_4/SiO_2 and Mn−Na_2WO_4/TiO_2.

For the used MNWS catalyst, the surface Si atomic concentration significantly increased, while the surface Na, Mn, and W contents significantly decreased. Literature[35] suggests that the decrease in Na and W in the MNWS catalyst system is due to leaching during the reaction. This study argues that the reduction in Na, W, and Mn concentration on the surface of the used MNWS catalyst is not due to leaching of these elements but rather the chemical reaction between SiO_2 and H_2O, inducing the migration of SiO_2 to the surface and covering part of the Na, W, and Mn originally on the surface. There are two pieces of evidence supporting this viewpoint: (1) Thermodynamic calculations, XRD, and *in situ* IR characterization all support the reaction between SiO_2 and H_2O at high temperatures, which would necessarily induce Si migration to the surface. (2) XPS analysis of steam-treated MNWT showed that although surface Na slightly decreased, W and Mn slightly increased, indicating no significant leaching of main active components.

These results demonstrate that the chemical reaction between SiO_2 and H_2O at high temperatures increases the surface Si content, covering parts of Na, W, and Mn, which is not observed for the TiO_2 support in MNWT. Consequently,

https://doi.org/10.1021/acsomega.4c05565
ACS Omega 2024, 9, 36751−36760

Table 4. XPS Element Binding Energy and Surface Atomic Concentration of the Fresh and Used (with H_2O) Mn−Na_2WO_4/SiO_2[a]

Name	Peak BE (eV)[b]	Assignments	Surface atomic concentration (at.%)	
			Fresh	Used with H_2O
Na 1s	1071.59, 1071.76	Na_2WO_4, Na_2SiO_3	7.24	6.72
W 4f7	35.35, 35.36	Na_2WO_4, $MnWO_4$	2.47	1.90
Mn 2p3	641.37, 641.47	MnO, $MnWO_4$	1.42	0.92
Si 2p	103.20, 103.11	SiO_2	22.90	26.87
O 1s(a)	530.29, 530.41	WO_4^{2-}, MnO	17.31	15.81
O 1s(b)	532.33, 532.36	SiO_2	41.14	45.92
O 1s(c)	535.07, 535.45	Adsorbed O	7.52	1.85

[a]Loading: 2.15 wt % Mn, 5.4 wt % Na_2WO_4 [b]Two number represent fresh and used respectively

Table 5. XPS Element Binding Energy and Surface Atomic Concentration of the Fresh and Used (with H_2O) Mn−Na_2WO_4/TiO_2[a]

Name	Peak BE (eV)[b]	Assignment	Surface atomic concentration (at.%)	
			Fresh	Used with H_2O
Na 1s	1071.44, 1071.29	Na_2WO_4	12.86	11.92
W 4f7	35.18, 35.22	Na_2WO_4	4.40	4.61
Mn 2p3	641.11, 641.22	MnO	1.06	1.27
Ti 2p3	457.77, 457.76	TiO_2	15.30	15.40
O 1s(a)	529.15, 529.19	TiO_2	30.30	30.91
O 1s(b)	530.52, 530.51	Na_2WO_4, MnO	30.76	32.75
O 1s(c)	534.37, 534.77	Adsorbed O	5.31	3.15

[a]Loading: 2.15 wt % Mn, 5.4 wt % Na_2WO_4 [b]Two number represent fresh and used, respectively

the surface concentration of the major elements in MNWT changes only slightly. This further confirms that the role of H_2O in the OCM reaction process differs significantly between MNWS and MNWT. For MNWS, H_2O participates in and promotes the oxidative coupling of methane, mainly by facilitating the activation and conversion of gas-phase molecular oxygen on the catalyst surface. In contrast, for MNWT, H_2O hinders the oxidative coupling of methane primarily by adsorbing on the surface and isolating the gas-phase molecular oxygen, thereby blocking its activation and conversion.

The O 1s spectra for MNWS and MNWT indicate three types of surface oxygen species: (1) Oxygen species of the support. For both catalysts, these are approximately double the amount of support elements Si (MNWS) and Ti (MNWT). Interestingly, the O 1s binding energy of Si−O in MNWS (∼532.3 eV) is about 2 eV higher than that combined with W and Mn (∼530.3 eV), whereas the O 1s binding energy of Ti−O in MNWT (∼529.2 eV) is about 1.3 eV lower than that combined with W and Mn (∼530.5 eV). Higher O 1s binding energy suggests lower valence electron density, implying a higher probability of participating in chemical reactions. This might be a key reason for the interaction between the support and H_2O in MNWS but not in MNWT. (2) Oxygen species of Na−O, W−O, and Mn−O. The surface atomic concentration of this oxygen species in used MNWS is about 16 at. %, roughly half of MNWT (∼32 at. %). The surface atomic concentrations of Na and W in MNWT are approximately twice that of MNWS, which may lead to stronger adsorption of H_2O on MNWT. This substantial surface adsorption of H_2O could hinder the activation of gas-phase molecular oxygen on surface Mn or W sites, possibly explaining the significant reduction in activity of MNWT upon the introduction of H_2O. (3) Surface adsorbed oxygen species. The surface adsorbed oxygen in used MNWS (1.85 at. %) is much lower than that in MNWT (3.15 at. %), positively correlating with the surface concentrations of W and Mn. This suggests that W and Mn on the surface are the main active sites for molecular oxygen adsorption and activation.

Figure 5(a) shows the results of the O_2-TPD for the MNWS and MNWT catalysts. Both catalysts exhibit no significant changes in the peak temperatures and initial temperatures of oxygen desorption before and after the reaction, indicating that the main oxygen species on the catalysts did not change significantly, consistent with the XPS characterization results. For MNWS, oxygen desorption begins at 690 °C and peaks at 923 °C, while for MNWT, desorption begins at 580 °C and peaks at 716 °C. This peak temperature difference aligns with the XPS results, indicating that the binding of W−O and Mn−O in MNWS (O 1s BE 530.41 eV) is stronger than that in

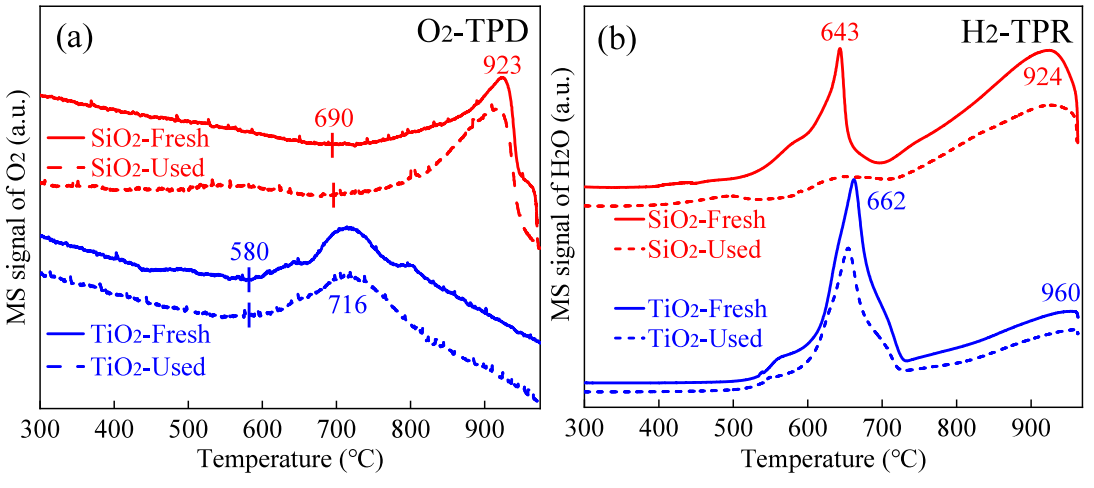

Figure 5. (a) O_2-TPD and (b) H_2-TPR profiles of the fresh and used (with H_2O) catalysts of Mn−Na_2WO_4/SiO_2 and Mn−Na_2WO_4/TiO_2.

https://doi.org/10.1021/acsomega.4c05565
ACS Omega 2024, 9, 36751−36760

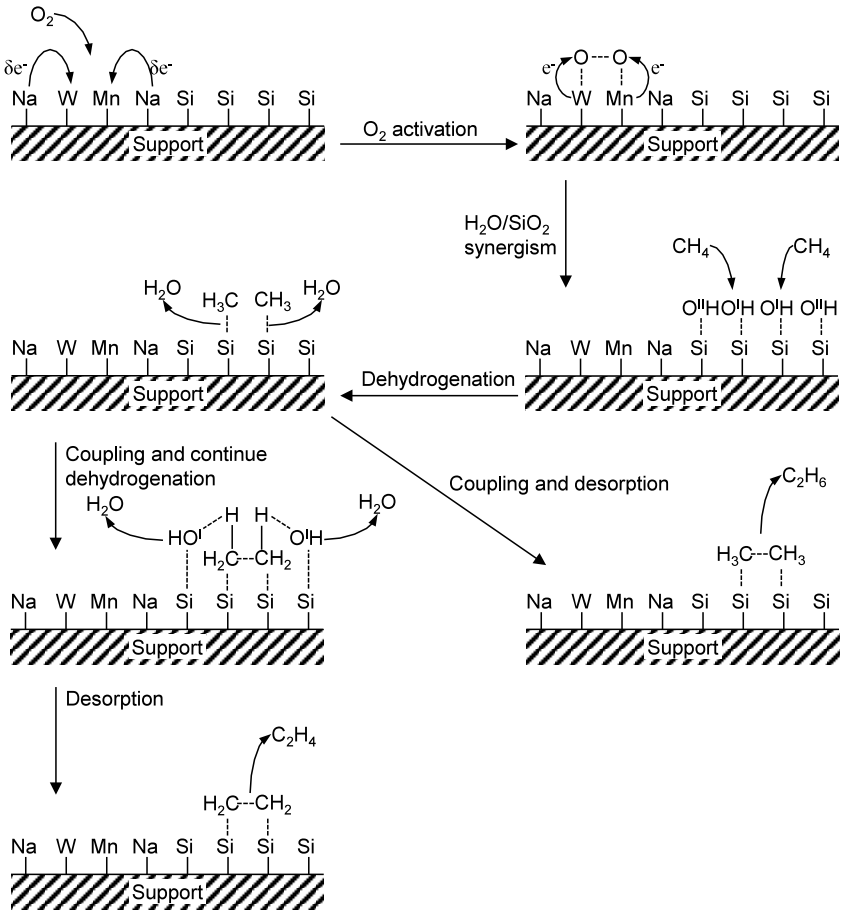

Figure 6. H_2O and SiO_2 synergetic promoted the OCM reaction mechanism model over the Mn−Na_2WO_4/SiO_2 catalyst.

MNWT (O 1s BE 530.51 eV). According to literature sources,[9,36] oxygen desorption peaks around 600 °C can be attributed to weakly bound lattice oxygen species with high oxygen atom mobility. This also explains the findings in literature,[37] where the Mn−Na_2WO_4/TiO_2 catalyst exhibits higher activity at lower temperatures, with a CH_4 conversion of 26% and C_{2+} selectivity of 76% at 720 °C. In contrast, the Mn−Na_2WO_4/SiO_2 catalyst shows a sharp decline in catalytic performance, with a CH_4 conversion of 7.2% and C_{2+} selectivity of 9.2% at 720 °C.

Figure 5(b) shows the H_2-TPR results for the MNWS and MNWT catalysts. Both catalysts exhibit two reduction peaks: the lower temperature peak corresponds to the reduction of MnO_x ($x > 1$) species, and the higher temperature peak corresponds to the reduction of Na-WO_x species.[19] For the fresh catalysts, the two reduction peak temperatures for the SiO_2-supported catalyst are both lower than those for the TiO_2-supported catalyst, indicating that the MnO_x and Na-WO_x species in the SiO_2-supported catalyst are more easily reduced. This suggests that the SiO_2-supported catalyst facilitates electron transfer through the redox cycling of valence-variable metals Mn and W during the OCM reaction, thereby activating the hydrocarbon reactants. For the MNWS catalyst, the reduction peak of the MnO_x species significantly decreases after the reaction, likely due to the reduced Mn content on the catalyst surface and the formation of more stable $MnWO_4$.

In summary, during the oxidative coupling of methane over the MNWS catalyst, electrons are primarily transferred through the valence metal W and Mn, particularly Mn^{2+}, which activates molecular oxygen (O_2) and subsequently activates CH_4. Sodium, as an alkali metal, acts as an electron donor promoter, enhancing the electron transfer capability of the catalyst and improving its intrinsic activity. Literature[38] has discussed the synergistic mechanism between Na, W, and Mn, but it has not addressed the roles of SiO_2 and H_2O. This study demonstrates the significant roles of SiO_2 and H_2O in promoting the OCM reaction. Based on the evaluation and characterization results, a more reasonable mechanism for the synergistic promotion of the OCM reaction by H_2O and SiO_2 in the MNWS system is proposed, as illustrated in Figure 6.

In this mechanism, after gas-phase molecular oxygen adsorbs on the MNWS surface, it gains $2e^-$ from the W and Mn sites, forming the compound O_2^{2-}. This species then migrates to adjacent Si sites and reacts with two H_2O molecules, forming two adjacent highly active surface hydroxyl radicals (O^IH) and two ordinary hydroxyl groups ($O^{II}H$) on two neighboring Si atoms. Two CH_4 molecules react with the two adjacent surface hydroxyl radicals (O^IH) to form two neighboring methyl groups (CH_3). These neighboring methyl groups can quickly couple to form C_2H_6. The surface CH_3 or C_2H_6 can further react with adjacent surface hydroxyl radicals (O^IH) to dehydrogenate and form C_2H_4. The ordinary hydroxyl groups ($O^{II}H$) can reversibly dehydrate at high temperatures to restore the surface SiO_2 structure. During the dehydrogenation of CH_4 or C_2H_6 by adjacent surface hydroxyl radicals (O^IH), the electron-deficient metals W and Mn gain electrons, reducing themselves and completing the catalytic redox cycle.

https://doi.org/10.1021/acsomega.4c05565
ACS Omega 2024, 9, 36751−36760

In this entire system, SiO_2 and H_2O play crucial roles in forming the dehydrogenation active sites, surface hydroxyl radicals (O^IH), which synergize with the synthesis of aqueous O_2^{2-} to facilitate the formation of hydrocarbon compounds.

4. CONCLUSION

Through the study of Mn−Na_2WO_4 catalysts supported on different supports, the results show that the Mn−Na_2WO_4/SiO_2 catalyst exhibits significantly better high-temperature (800 °C) catalytic performance compared with other supports. The introduction of steam into the feedstock further enhances the catalytic activity and selectivity. Based on thermodynamic calculations and characterization, the following conclusions are drawn:

(1) Thermodynamic calculations and characterization analyses support that there is a chemical reaction between SiO_2 and H_2O at high temperatures, which can generate surface adjacent disilanol groups.
(2) Gas-phase molecular oxygen primarily gains electrons through variable-valence metals Mn and W, forming intermediate oxygen species O_2^{2-}. These intermediate oxygen species react with H_2O and SiO_2 through synergistic effects, forming adjacent surface disilanol radical active sites.
(3) The adjacent surface disilanol radicals are the active sites for the dehydrogenation of CH_4 and C_2H_6. The introduction of steam promotes the formation of these disilanol active sites, thereby significantly improving both the CH_4 conversion and C_{2+} selectivity in the oxidative coupling of methane.

AUTHOR INFORMATION

Corresponding Author

Changchun Yu − *College of New Energy and Materials, China University of Petroleum, Beijing 102249, P. R. China;* orcid.org/0000-0002-7973-6859; Email: yucc@cup.edu.cn

Authors

Qingjing Liu − *State Key Laboratory of Heavy Oil Processing, China University of Petroleum, Beijing 102249, P. R. China;* orcid.org/0009-0004-0417-9308

Ruisheng Wang − *College of New Energy and Materials, China University of Petroleum, Beijing 102249, P. R. China*

Ranjia Li − *College of New Energy and Materials, China University of Petroleum, Beijing 102249, P. R. China*

Xiaosheng Wang − *College of New Energy and Materials, China University of Petroleum, Beijing 102249, P. R. China;* orcid.org/0000-0003-3389-4031

Suoqi Zhao − *State Key Laboratory of Heavy Oil Processing, China University of Petroleum, Beijing 102249, P. R. China;* orcid.org/0000-0003-3707-2844

Complete contact information is available at: https://pubs.acs.org/10.1021/acsomega.4c05565

Notes

The authors declare no competing financial interest.

ACKNOWLEDGMENTS

This work was supported by the National Natural Science Foundation of China (Grant No. 21961132026). During the preparation of this work, the authors used OpenAI's ChatGPT in order to improve the writing and grammar. After using this tool, the authors reviewed and edited the content as needed and take full responsibility for the content of the publication.

REFERENCES

(1) Keller, G Synthesis of ethylene via oxidative coupling of methane I. Determination of active catalysts. *J. Catal.* **1982**, *73* (1), 9−19.
(2) Lunsford, J. H. Catalytic conversion of methane to more useful chemicals and fuels: a challenge for the 21st century. *Catal. Today* **2000**, *63*, 165−174.
(3) Olivos Suarez, A. I.; Szécsényi, A.; Hensen, E. J. M.; Ruiz-Martínez, J.; Pidko, E. A.; Gascon, J. Strategies for the Direct Catalytic Valorization of Methane Using Heterogeneous Catalysis: Challenges and Opportunities. *ACS Catal.* **2016**, *6* (5), 2965−2981.
(4) Gao, Y.; Neal, L.; Ding, D.; Wu, W.; Baroi, C.; Gaffney, A. M.; Li, F. Recent Advances in Intensified Ethylene Production–A Review. *ACS Catal.* **2019**, *9* (9), 8592−8621.
(5) Fang, X. Preparation and characterization of catalysts for methane oxidative coupling. *J. Gannan Normal Univ.* **1992**, *3*, 69−77.
(6) Fang, X.; Li, S.; Lin, J.; Gu, J.; Yang, D. Preparation and characterization of catalysts for oxidative coupling of methane. *Mol. Catal. (China)* **1992**, *6* (4), 255−261.
(7) Fang, X.; Li, S.; Lin, J.; Chu, Y. Oxidative coupling of methane on W-Mn catalysts. *Mol. Catal. (China)* **1992**, *6* (6), 427−433.
(8) Arndt, S.; Otremba, T.; Simon, U.; Yildiz, M.; Schubert, H.; Schomaecker, R. Mn-Na_2WO_4/SiO_2 as catalyst for the oxidative coupling of methane. What is really known? *Applied Catalysis A: General* **2012**, *425*−*426*, 53−61.
(9) Jeon, W.; Lee, J. Y.; Lee, M.; Choi, J. W.; Ha, J. M.; Suh, D. J.; Kim, W. Oxidative coupling of methane to C_2 hydrocarbons on the Mg-Ti mixed oxide-supported catalysts at the lower reaction temperature: Role of surface oxygen atoms. *Applied Catalysis A: General* **2013**, *464*−*465*, 68−77.
(10) Wang, J.; Chou, L.; Zhang, B.; Song, H.; Zhao, J.; Yang, J.; Li, S. Comparative study on oxidation of methane to ethane and ethylene over Na_2WO_4-Mn/SiO_2 catalysts prepared by different methods. *J. Mol. Catal. A: Chem.* **2006**, *245* (1−2), 272−277.
(11) Wang, P.; Zhang, X.; Zhao, G.; Liu, Y.; Lu, Y. Oxidative coupling of methane: MO_x-modified (M = Ti, Mg, Ga, Zr) Mn_2O_3-Na_2WO_4/SiO_2 catalysts and effect of MO_x modification. *Chinese Journal of Catalysis* **2018**, *39* (8), 1395−1402.
(12) Hayek, N. S.; Khlief, G. J.; Horani, F.; Gazit, O. M. Effect of reaction conditions on the oxidative coupling of methane over doped MnO_x-Na_2WO_4/SiO_2 catalyst. *J. Catal.* **2019**, *376*, 25−31.
(13) Sadjadi, S.; Simon, U.; Godini, H. R.; Gorke, O.; Schomacker, R.; Wozny, G. Reactor material and gas dilution effects on the performance of miniplant-scale fluidized-bed reactors for oxidative coupling of methane. *Chemical Engineering Journal* **2015**, *281*, 678−687.
(14) Gordienko, Y.; Usmanov, T.; Bychkov, V.; Lomonosov, V.; Fattakhova, Z.; Tulenin, Y.; Shashkin, D.; Sinev, M. Oxygen availability and catalytic performance of NaWMn/SiO_2 mixed oxide and its components in oxidative coupling of methane. *Catal. Today* **2016**, *278*, 127−134.
(15) Wang, D. J.; Rosynek, M. P.; Lunsford, J. H. Oxidative coupling of methane over oxide-supported sodium-manganese catalysts. *J. Catal.* **1995**, *155*, 390−402.
(16) Ji, S.; Li, S. Study on methane activation over Na-W-Mn/SiO_2 catalysts I structure of the active center. *Mol. Catal. (China)* **2000**, *14* (1), 5.
(17) Jiang, Z.; Gong, H.; Li, S. Methane activation over Mn_2O_3-Na_2WO_4/SiO_2 catalyst and oxygen spillover spillover. *Stud. Surf. Sci. Catal.* **1997**, *112*, 481.
(18) Li, S. Oxidative Coupling of Methane over W-Mn/SiO_2 Catalyst. *Chin. J. Chem.* **2001**, *19* (1), 16−21.
(19) Sourav, S.; Kiani, D.; Wang, Y.; Baltrusaitis, J.; Fushimi, R. R.; Wachs, I. E. Molecular structure and catalytic promotional effect of

https://doi.org/10.1021/acsomega.4c05565
ACS Omega 2024, 9, 36751−36760

Mn on supported Na_2WO_4/SiO_2 catalysts for oxidative coupling of methane (OCM) reaction. *Catal. Today* **2023**, *416*, 113837.
(20) Kiani, D.; Sourav, S.; Wachs, I. E.; Baltrusaitis, J. Synthesis and molecular structure of model silicasupported tungsten oxide catalysts for oxidative coupling of methane (OCM). *Catalysis Science & Technology* **2020**, *10*, 3334−3345.
(21) Sourav, S.; Wang, Y.; Kiani, D.; Baltrusaitis, J.; Fushimi, R. R.; Wachs, I. E. New mechanistic and reaction pathway insights for oxidative coupling of methane (OCM) over supported Na_2WO_4/SiO_2 catalysts. *Angew. Chem., Int. Ed. Engl.* **2021**, *60* (39), 21502−21511.
(22) Sourav, S.; Wang, Y.; Kiani, D.; Baltrusaitis, J.; Fushimi, R. R.; Wachs, I. E. Resolving the types and origin of active oxygen species present in supported Mn-Na_2WO_4/SiO_2 catalysts for oxidative coupling of methane. *ACS Catal.* **2021**, *11* (16), 10288−10293.
(23) Sinev, M.; Ponomareva, E.; Sinev, I.; Lomonosov, V.; Gordienko, Y.; Fattakhova, Z.; Shashkin, D. Oxygen pathways in oxidative coupling of methane and related processes. Case study: NaWMn/SiO_2 catalyst. *Catal. Today* **2019**, *333*, 36−46.
(24) Fleischer, V.; Simon, U.; Parishan, S.; Colmenares, M. G.; Gorke, O.; Gurlo, A.; Riedel, W.; Thum, L.; Schmidt, J.; Risse, T.; et al. Investigation of the role of the $Na_2WO_4/Mn/SiO_2$ catalyst composition in the oxidative coupling of methane by chemical looping experiments. *J. Catal.* **2018**, *360*, 102−117.
(25) Fleischer, V.; Steuer, R.; Parishan, S.; Schomacker, R. Investigation of the surface reaction network of the oxidative coupling of methane over $Na_2WO_4/Mn/SiO_2$ catalyst by temperature programmed and dynamic experiments. *J. Catal.* **2016**, *341*, 91−103.
(26) Takanabe, K.; Iglesia, E. Rate and selectivity enhancements mediated by OH radicals in the oxidative coupling of methane catalyzed by $Mn/Na_2WO_4/SiO_2$. *Angew. Chem.* **2008**, *120* (40), 7803−7807.
(27) Takanabe, K.; Khan, A. M.; Tang, Y.; Nguyen, L.; Ziani, A.; Jacobs, B. W.; Elbaz, A. M.; Sarathy, S. M.; Tao, F. Integrated in situ characterization of a molten salt catalyst surface: evidence of sodium peroxide and hydroxyl radical formation. *Angew. Chem., Int. Ed.* **2017**, *56* (35), 10403−10407.
(28) Ji, S.-f.; Xiao, T.-c.; Li, S.-b.; Xu, C.-z.; Hou, R.-l.; Coleman, K. S; Green, M. L.H The relationship between the structure and the performance of Na-W-Mn/SiO_2 catalysts for the oxidative coupling of methane. *Appl. Catal., A* **2002**, *225*, 271−284.
(29) Chen, H.; Niu, J.; Zhang, B.; Li, S. Synergic effect of active components in Na-W-Mn/SiO_2 catalyst. *Chin. J. Catal.* **2000**, *21* (1), 55−58.
(30) Guillaumont, R.; Fanghänel, T.; Fuger, J.; Grenthe, I.; Neck, V.; Palmer, D. A.; Rand, M. H. *Update on the Chemical Thermodynamics of U, Np, Pu, Am and Tc, Chemical Thermodynamics*; Mompean, F. J., Illemassene, M., Domenech-Orti, C., Ben Said, K., Eds.; Elsevier, 2003; Vol. *5*.
(31) Yungman, V. S.; Glushko, V. P.; Medvedev, V. A.; Gurvich, L. V. *Thermal Constants of Substances*; New York, 1999.
(32) Bailey, S. M.; Churney, K. L.; Nuttall, R. L. The NBS Tables of Chemical Thermodynamic Properties, Selected Values for Inorganic and C1 and C2 Organic Substances in SI Units. *J. Phys. Chem. Ref. Data*, **1982**, *11*, 1−392.
(33) Chuang, I. S.; Maciel, G. E. A detailed model of ocal structure and silanol hydrogen bonding of silica gel surfaces. *J. Phys. Chem. B* **1997**, *101*, 3052−3064.
(34) Chuang, I. S.; Maciel, G. E. Probing hydrogen bonding and the local environment of silanols on silica surfaces via nuclear spin cross. *J. Am. Chem. Soc.* **1996**, *118*, 401−406.
(35) Lin, J.; Chu, Y.; Gu, J.; Yang, D.; Zhang, C.; Yang, Y.; Li, S. Loss of Na_2WO_4 and its influence on the oxidative coupling of methane on W-Mn/SiO_2 catalyst. *Mol. Catal. (China)* **1996**, *10* (3), 194−200.
(36) Sun, W.; Gao, Y.; Zhao, G.; Si, J.; Liu, Y.; Lu, Y. Mn_2O_3-Na_2WO_4 doping of $Ce_xZr_{1-x}O_2$ enables increased activity and selectivity for low temperature oxidative coupling of methane. *J. Catal.* **2021**, *400*, 372−386.
(37) Wang, P.; Zhao, G.; Wang, Y.; Lu, Y. $MnTiO_3$-driven low-temperature oxidative coupling of methane over TiO_2-doped Mn_2O_3-Na_2WO_4/SiO catalyst. *Sci. Adv.* **2017**, *3*, e1603180.
(38) Kiani, D.; Sourav, S.; Baltrusaitis, J.; Wachs, I. E. Oxidative coupling of methane (OCM) by SiO_2-supported tungsten oxide catalysts promoted with Mn and Na. *ACS Catal.* **2019**, *9* (7), 5912−5928.

https://doi.org/10.1021/acsomega.4c05565
ACS Omega 2024, 9, 36751−36760